PNAS
www.pnas.org

Supplementary Information for

β-arrestin-dependent PI(4,5)P_2 synthesis boosts GPCR endocytosis

Seung-Ryoung Jung, Yifei Jiang, Jong Bae Seo, Daniel T. Chiu, Bertil Hille, and Duk-Su Koh

Corresponding author: Seung-Ryoung Jung

Email: jsr007@uw.edu

This PDF file includes:

Supplementary Discussion of Fig. S2

The roles of PI(4)P pools in restoration of $PI(4,5)P_2$ was examined with two pharmacological blockers of the synthesis of PI(4)P from PI: i) wortmannin (Fig. S2A), a general blocker of PI4KIII (1) and ii) BAPTA-AM (Fig. S2B), a Ca^{2+} chelator that slows the Ca^{2+}-dependent PI4KIII (2, 3). Application of either agent initiated a slow and spontaneous rundown of the PI(4)P pools (Fig. S2A and B, green); the PH-RFP probe (magenta) did not report any change, but its relatively high affinity to PM $PI(4,5)P_2$ might have masked a partial loss. Activation of PAR2 with AP depleted PM $PI(4,5)P_2$ strongly and, after a short delay, PI(4)P as well. Gradually there was a partial recovery of the $PI(4,5)P_2$ signal, but hardly any recovery of PI(4)P. Neither signal showed the complete recovery observed in control cells (Fig. 1B).

In addition, we tested two perturbants of membrane trafficking and delivery of PI(4)P from the Golgi to the PM (1): i) blebbistatin (Fig. S2C), an inhibitor of myosin II and of the budding from the Golgi membrane (4) and ii) brefeldin A (Fig. S2D), which disrupts the Golgi apparatus (5). These two agents initiated only a small spontaneous loss of total PI(4)P, but after application of AP, the changes of PI(4)P and $PI(4,5)P_2$ were similar to those with reduced PI4K enzyme activity (Fig. S2A and B). Thus, preventing synthesis or delivery of PI(4)P to the PM leads to a correlated deficit in the recovery of PM $PI(4,5)P_2$ after PAR2 activation (Fig. 1C, Pearson's correlation coefficient, 0.85).

Supplementary Methods and Materials

Cell culture: HEK-cell-derived tsA201 cells (Sigma-Aldrich) were cultured in Dulbecco's Modified Eagle Medium (DMEM) supplemented with 10% fetal bovine serum and 1% penicillin and streptomycin. Single cells were plated on 5 mm glass chips for the confocal imaging, FRET and PAR2-endocytosis assay, and on 25 mm round coverslips for conventional and single-molecule TIRF experiments. The glass was coated with poly-L-ornithine (0.1 mg/ml, Sigma-Aldrich) except in the single-molecule TIRF and direct STORM imaging experiments (1 mg/ml poly-L-ornithine). All experiments were performed at room temperature (22-24^{o}C).

Materials and solutions: Blebbistatin was purchased from EMD Biosciences (MA) and Brefeldin A and Wortmannin were from Sigma-Aldrich. Rapamycin and activating peptide (AP, six amino acid peptide: N-SLIGKT-C) were from LC Laboratories (MA) and United Biosystems (United Biosystems Inc. VA), respectively. Clathrin heavy chain siRNA (Cat#: sc-35067) and primary antibody for immunocytochemistry (Cat #: sc-12734) were purchased from Santa Cruz, Inc. Control siRNA was the same as previously used and tested (6). Bodipy-$PI(4,5)P_2$ was from Echelon Biosciences (Cat#: C-45F6). Barbadin was from Medchemexpress LLC (Cat#: HY-119706) and Pitstop2 was from Abcam (Cat#: ab120687). Saline solution contained (mM): 137.5 NaCl, 2.5 KCl, 1 $MgCl_2$, 2 $CaCl_2$, 10 glucose, and 10 HEPES (pH adjusted to 7.2 with NaOH).

Transfection of cDNA: tsA201 cells were transfected with cDNA (~0.5 µg per 35 mm dish) and X-tremegene 9 (10 µl, Roche Applied Science, IN) according to the manufacturer's protocol. Right after incubation for 4-5 hours with the different combinations of cDNA, cells were treated with 0.05% trypsin, transferred onto glass chips, and incubated for one day prior to imaging. For Golgi localization of Sac1,

we chose cells minimally overexpressing TGN38, Giantin, and Sac1 constructs (~ 0.25 µg cDNA per 35 mm dish) to reduce the mislocalization of Sac1 to the PM after treatments with rapamycin. For PM-localization of Sac1, we selected cells with LDR-CFP localized at the PM and only moderate expression of RFP-Sac1. For PH-RFP and GFP-P4M probes, 0.3 µg cDNA constructs were transfected. PH-GFP and PH-RFP, were kindly provided by Chris Kearn (University of Washington, Seattle, WA), GFP-P4M by Gerald Hammond (University of Pittsburgh, reference 7); and human PAR2-GFP, by Nigel Bunnett (Monash Institute of Pharmaceutical Sciences, Parkville, VIC, Australia). PAR2-dark (6) was subcloned into pcDNA3.1 (Invitrogen, Life technologies, NY). For the rapamycin-induced translocations, monomeric RFP-tagged human Sac1 (RFP-Sac1-FKBP) and TGN38-FRB-CFP were obtained from Tamas Balla (National Institutes of Health (NIH)) and Giantin-FRB-CFP from Takanari Inoue (Johns Hopkins University). We used lyn11-FRB-CFP (LDR-CFP) and Inp54p 5-phosphatase (recruitable 5-phosphatase) as described in our previous studies (1, 8). The clathrin-DsRed ('clathrin light chain-DsRed') was obtained from Liangyi Chen (Peking University) with permission from Thomas Kirchhausen (Harvard University, Ehrlich et al., 2004). GFP tagged human PIP5K-Iγ p87 (De Camilli lab construct) for the Fig. 4F-G was obtained from Addgene (cat#: 22300). We used our engineered CFP tagged murine PIP5K-Iγ (CFP-PIP5K) for the Fig. 4H (8), which localizes in the cytosolic compartment. Wild type bovine β-arrestin-2-YFP was from Martin Lohse (University of Würzburg, Germany), and wild type rat β-arrestin-2-mRFP was used for Fig. 4F-G. We made new constructs for the KRK and KK mutants of bovine β-arrestin-2-YFP and KRK mutant of bovine β-arrestin-2-mRFP.

Fluorescence resonance energy transfer (FRET). Briefly, epifluorescence photometry was used to measure the FRET between CFP and YFP (9). Emission light from CFP and YFP were collected by photomultipliers in photon-counting mode using an inverted Nikon Diaphot microscope equipped with a 40X 1.3 NA oil-immersion objective. CFP was excited at 440 nm and emissions for CFP and YFP were collected at 480 nm and 535 nm, respectively. The FRET ratio (FRETr) was taken as the ratio of YFP emission divided by CFP emission after correction for background and bleed-through (9). FRETr values collected at 1 Hz were normalized to the control value before treatment with agonist to remove cell-to-cell variation.

Confocal microscopy: Confocal images were taken every 12 or 22 s with a Zeiss 710 Confocal microscope. Excitation wavelengths were 488 nm for GFP (Argon laser), 561 nm for RFP (diode-pumped solid-state laser), and 633 nm for Alexa647 dye (helium-neon laser). Emitted fluorescence was collected *via* a 40X oil immersion lens (N.A. 1.3). Agonist and drugs were applied to the bath. The images were analyzed with ImageJ (National Institutes of Health). When imaged cells were patch clamped to measure activity of PIP5-kinase using VSP, the cell membrane was held at –60 mV. To activate VSP, the voltage was jumped from –60 to +100 mV for 2 s while $PI(4,5)P_2$ was monitored with the PH-RFP probe (Fig. 4). For clathrin heavy chain siRNA experiments (Fig. 6I), cells were transfected with clathrin heavy chain siRNAs or with control siRNA for 4 h and then PAR2-GFP and PH-RFP cDNAs were added in the presence of the siRNAs for 4-5 h of additional incubation. We performed immunocytochemistry with monoclonal primary antibody conjugated with Alexa647 dye to measure endogenous clathrin heavy chains after knockdown with the clathrin heavy chain siRNA (*SI Appendix* Fig. S14A). Briefly, after cells were fixed with 4% paraformaldehyde for 10 min, the cell membrane was permeabilized with 0.1% Triton-X 100 for 15 min. Then cells were incubated with 1% BSA for 20 minutes to minimize non-specific

binding of primary antibody. The primary antibody was introduced for 15 min and then washed out with the saline solution. Before confocal experiments, we waited for 1 day to eliminate free antibodies from inside the cells at 4 ^{o}C. We then measured the cytosolic intensity of the primary antibody and quantified with ImageJ.

Conventional TIRF microscopy: Conventional total internal reflection fluorescence (TIRF) microscope used a Nikon TE inverted microscope and an APO TIRF 63X/1.49 objective lens (Nikon, Japan). Every 7 s, a consecutive pair of images was recorded with the 488 and 561 nm lasers for GFP and RFP proteins, respectively. The time lag between 488 and 561 nm lasers was less than 2 s. The images were collected by a QuantEM camera (Photometrics Technology, AZ) and analyzed with ImageJ. Because the endocytosis mechanism is sensitive to membrane tension, we used a lower concentration of poly L-ornithine (0.1 mg/ml) for coating the cover glasses than was used in the single-molecule tracking experiments.

Single-molecule live-cell imaging with TIRF microscopy: To produce flat cells for visualizing PAR2-CCP interaction at single-molecule sensitivity, #1 25 mm cover glasses were coated with 1 mg/ml poly L-ornithine for at least 60 min, which strengthened the adhesion of cell membranes to the glass surface. The background signal from organic molecules bleached within a few seconds after the first exposure to laser light. PAR2 receptors were labeled with Alexa647-labeled primary antibody for 5-15 min. The remaining free antibody was washed out three times with saline solution. SNAP-tag labeling was performed as published (9, 10). Briefly, for Fig. 6B-D, cells were transiently transfected with plasmids for PAR2-dark (0.1-0.15 μg cDNA) and SNAP-tagged clathrin light chain (CLC) (SNAP-CLC-SNAP, 0.05-0.1 μg, Addgene number 38012). After one day, cells were incubated with 2.5 μM cell-permeable SNAP-cell 505-star dye (New England Biolabs Inc., MA) for 45 min in cell culture medium in a 37^{o}C CO_2 incubator and then washed three times with culture medium. To slow photobleaching of Alexa647 dyes conjugated to the PAR2 primary antibody, an oxygen scavenger system was used in the presence of metabolites including α-ketoisocaproate (10 mM) and glutamine (2 mM) to minimize ATP depletion during low oxygen (11). Single-molecule TIRF images were taken on a custom-built microscope based on a Nikon Eclipse TE2000 microscope base with an APO TIRF 100X/1.49 N.A. objective. A 641 nm laser was used for the illumination. Images were collected by an EMCCD ixon897 camera (Andor) and a custom controller written in LabVIEW (11). Dual-color imaging used two excitation lasers (488 and 641 nm) and two EMCCD cameras collecting emission at the same time. Multi-fluorescence solid latex beads (0.2 μm, Polysciences, PA, USA) were used for correcting registration errors (*SI Appendix* Fig. S13) of the two cameras in ImageJ and for NND analysis (*SI Appendix* Fig. S17).

To estimate diffusion coefficients, we used a Matlab program that tracked single PAR2 molecules (11). Our method was validated by tracking single lipid molecules on a ~100 nm liposome that mimicked CCPs of 100-200 nm diameter (12, 13). Here we reconstituted Cy5-conjugated phosphatidylethanolamine (Cy5-PE) into a palmitoyl-oleoyl-phosphatidylcholine (POPC) liposome (*SI Appendix* Fig. S10; see next section "POPC liposome reconstitution with Cy5-PE"). We were able to track single Cy5-PEs on the liposome with 10-20 nm localization precision using single-molecule localization TIRF microscopy (*SI Appendix* Fig. S11). For Fig. S15C-D, we also measured the mobility of Bodipy-PI(4,5)P_2 on lipid bilayers. The lipid bilayer was prepared on a glass surface using POPC liposomes, which fuse with the glass surface spontaneously. After 10 min, a uniform lipid bilayer had formed, and residual liposomes were washed out.

Then, a very small amount of Bodipy-PI(4,5)P_2 (100 ng/ml) was introduced onto the POPC lipid bilayer. Single molecule diffusion of the Bodipy-PI(4,5)P_2 at the lipid bilayer was analyzed with the same tracking algorithm as used for PAR2.

POPC liposome reconstitution with Cy5-PE: The lipids were supplied in chloroform solution. The POPC (Avanti, Cat# 850457C, 10 mg/ml) was divided into ~30 µl stock aliquots with ~0.3 mg of POPC. Biotin-PE was mixed with the one of the POPC stocks in a 40:1 ratio and then the chloroform was evaporated with nitrogen to make a lipid cake in a glass tube. Next, the Cy5-phosphatidylethanolamine (PE) (Avanti, Cat# 850457C, 1 mg/ml) and DiO (1 mg/ml) were each diluted 5000-fold in chloroform. 1 µl of the diluted Cy5-PE and 50 µl of the diluted DiO were added into the POPC/biotin-PE lipid cake. After the four lipids were thoroughly mixed, the chloroform was evaporated again. About 0.3 ml HEPES buffered solution (pH 7.3) was added to the lipid mixture (~0.3 mg/0.3 ml = 1 mg/ml) and vortexed until the solution looked milky. Then the solution was sonicated with a micro-tip under low power (20% duty cycle and power step 1, Branson Sonifier 450) for 30 s. The size of liposomes (measured by a dynamic light scattering DLS spectrometer, Malvern Zetasizer Nano ZS, Worcestershire, United Kingdom) depended on the parameters and varied batch-to-batch. Therefore, we used only a single batch for the experiment in *SI Appendix* Fig. S10. For selective immobilization of the biotin-conjugated liposomes, PEG/streptavidin was used to coat glass slides as described previously (14). A polydimethylsiloxane (PDMS)-based six-well mold was glued to the slide with epoxy. Finally, the prepared liposome samples were added into individual wells and held for a few minutes until the vesicles were immobilized on the glass. The residual liposomes were washed away with a HEPES buffer to reduce background signals.

Nearest neighbor distance (NND) analysis using single-molecule TIRF microscopy: NND analysis between species A and B compiles the center-to-center distances from each A to the closest neighboring B. Cells were transiently transfected with multiple combinations of cDNAs depending on the experiment as described in the figure captions. To reduce the density of expressed proteins, cells were transfected with 10~50-fold lower cDNA amounts than used for normal TIRF experiments. After confirming that we could see single-molecule diffusion of the proteins, we took images at 10 Hz frame rates for 100 s. Then the distance from each GFP-PIP5K-Iγs to the closest CCP or β-arrestin 2 was computed using the ThunderSTORM implanted in the ImageJ. This algorithm localizes centroids of individual GFP-PIP5K-Iγ molecules. The localized spots were collapsed onto a two-dimensional (2D) plane. Similarly, CCPs were localized to obtain their centroid positions. The two collapsed images were then merged after correction for registration errors defined by multi-color beads. For the NND analysis, we used the 'Spatial Statistics 2D/3D' implemented in ImageJ. The CCP image was used as a mask channel to filter the PIP5K-Iγ images ('F-function' in the algorithm). A distribution of virtual random spots of PIP5K-Iγs within a single CCP was simulated for comparison with real events of GFP-PIP5K-Iγ inside CCPs.

Direct STORM (dSTORM) imaging: Cells were transiently transfected with PAR2-dark in a 35 mm dish and transferred onto #1.5 rectangular cover glasses coated with poly-L-ornithine (1 mg/ml). Cells were cultured overnight prior to experiments. After activation of PAR2 with 100 µM activating peptide for 10 min, cells were fixed with 4% paraformaldehyde, permeabilized with 0.1% Triton X-100, and treated with 1% BSA for blocking. Endogenous β-arrestin 2 was labeled with primary antibody (1 µg/ml, Santa Cruz Inc.) in the presence of 1% BSA. Cells were thoroughly washed with 1% BSA solution without primary antibody. Alexa647-conjugated secondary antibody (5 µg/ml) was applied for 30 min. After

washing the cells with 1% BSA solution, dSTORM buffer was added into the imaging chamber. The buffer contained 100 mM Tris-HCl (pH 8.0), 1% glucose, 100 mM β-mercaptoethanol (BME), and oxygen scavengers (0.2 mg/ml catalase, 0.8 mg/ml pyranose 2-oxidase). dSTORM images were acquired with TIRF based STORM microscopy. A 640 nm laser was used for excitation and a 660-700 nm band pass filter for emission. An sCMOS camera collected images at 20 Hz. A 405 nm laser was occasionally used to activate Alexa647 dyes during the dSTORM imaging. The images were analyzed with ThunderSTORM in ImageJ (15).

PAR2 endocytosis assay: tsA201 cells transfected with PAR2-GFP were labeled intravitally with extracellular PAR2-primary antibody conjugated with Alexa647 dye (SAM11, Santa Cruz Inc.) for 15 min. Constitutive receptor internalization during this incubation was not significant. Internalization of PAR2 was slow and partial, so it was monitored after 1 h incubation to identify internalized granules or endosomes. Right after the antibody labeling, one batch of cells was fixed with 4% formaldehyde for 10 min and inspected with a Zeiss 710 confocal microscope; this allowed determination of the background fluorescence of the cytoplasm as an initial baseline. The remaining unfixed cells were treated with antibody-free drug solutions for the indicated time to allow receptor internalization and then fixed. Cytoplasmic and total intensities of the antibody were determined with ImageJ. Relative internalization of PAR2 was calculated from the ratio of cytoplasmic to total intensity of the antibody in each cell after subtracting the initial baseline fluorescence.

Data analysis: We used Igor 6.02 and Origin 8.5 to analyze and plot data.

Supplementary Figures

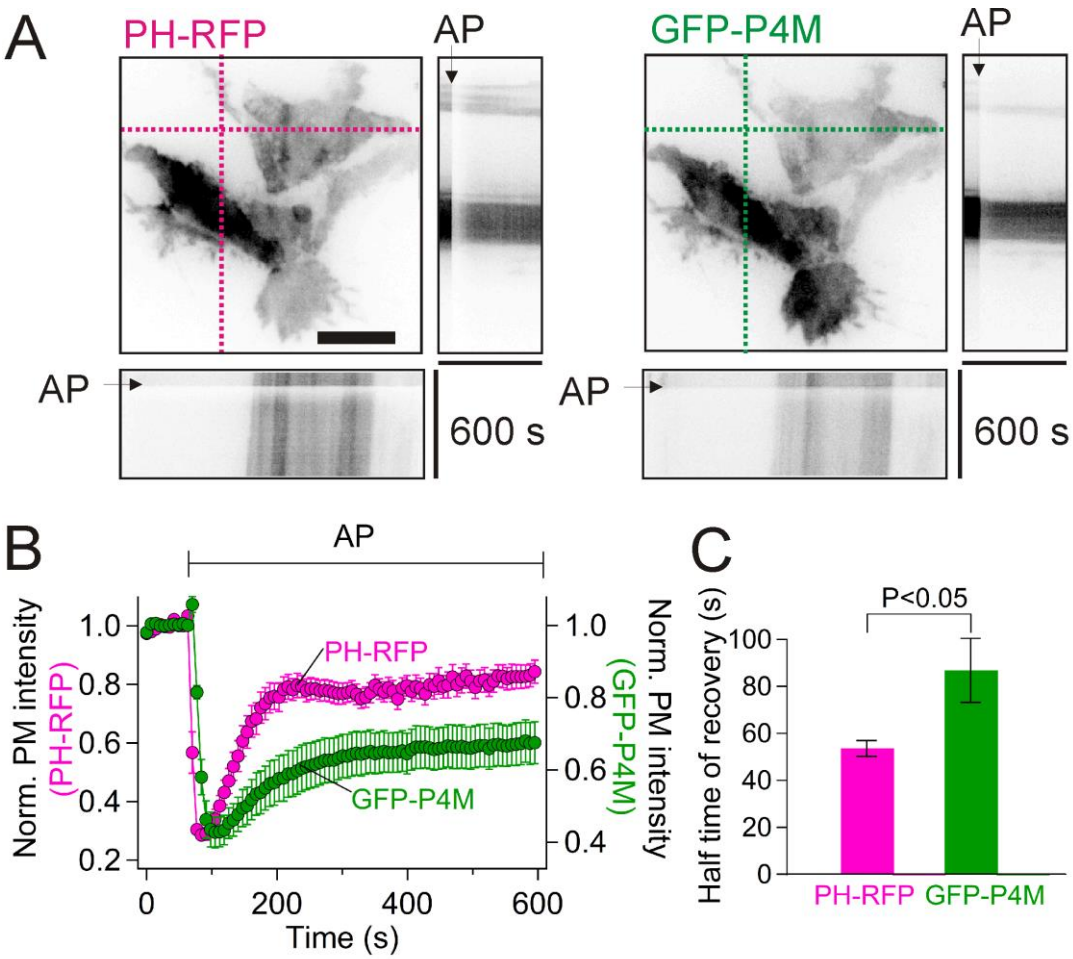

Fig. S1. Monitoring PI(4,5)P_2 (by PH-RFP probe) and PI(4)P (by GFP-P4M probe) at the plasma membrane (PM) using two-color conventional TIRF microscopy. (A) The first TIRF images (inverted contrast) of a time series with PH-RFP and GFP-P4M. Kymograph analysis was used to estimate time-dependent intensity changes in space. The magenta and green dotted lines in the TIRF images indicate the scan line used to determine intensities of the PH-RFP and GFP-P4M signals, respectively. The kymograph trace obtained from the horizontal magenta dotted lines in PH-RFP image is plotted below, with time advancing downward. Another kymograph trace from the vertical dotted line is plotted to the right of the TIRF image with time advancing to the right. The time for 100 µM AP application is indicated in both kymographs by arrows. Same for GFP-P4M image. Image scale bar, 10 µm. (B) Normalized time course of probe intensity at the plasma membrane (TIRF) before and after application of AP (n = 9 cells). (C) Half time of PI(4,5)P_2 (PH-RFP) and PI(4)P (GFP-P4M) recovery during AP treatment.

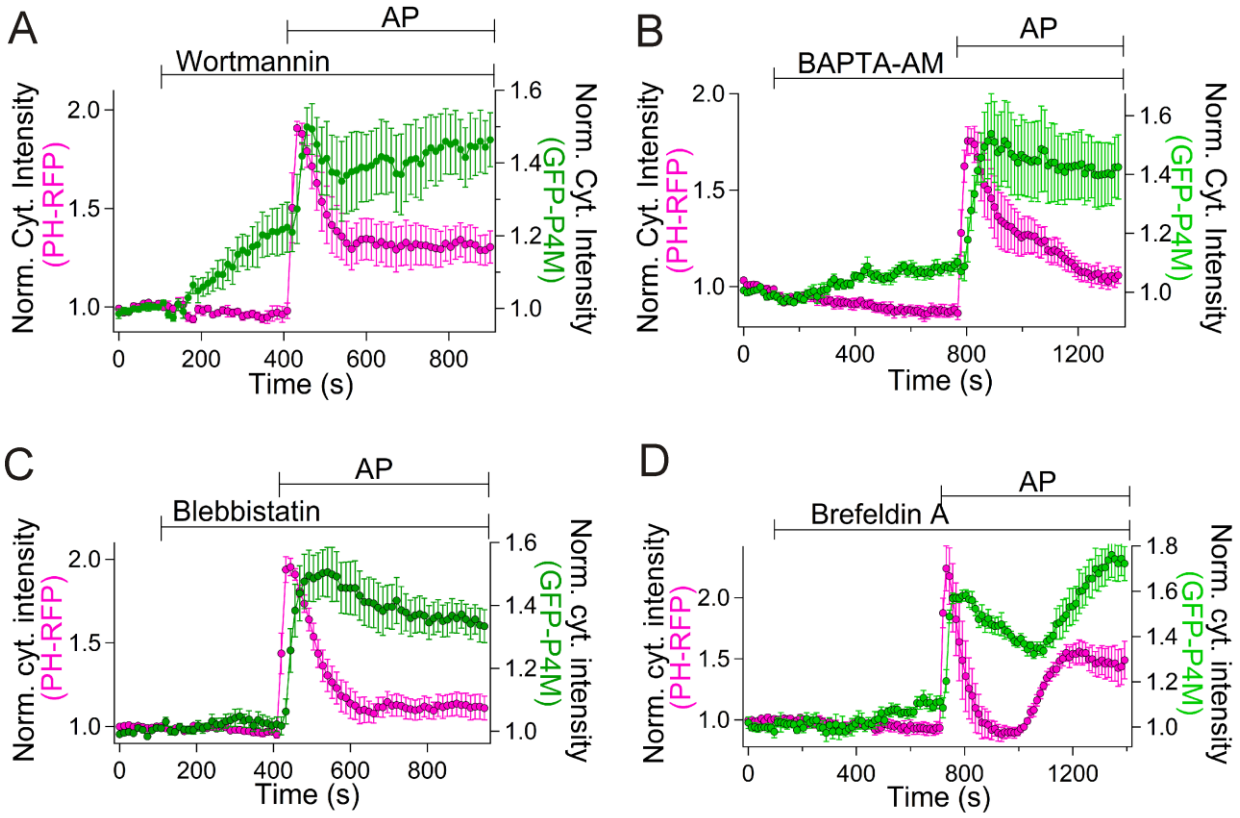

Fig. S2. Evidence of kinetic coupling between PI(4)P and PI(4,5)P_2 pools. Normalized intensity of PH-RFP and GFP-P4M probes in a cytoplasmic region of interest during treatment with 100 µM AP in the presence of: wortmannin (30 µM, A), BAPTA-AM (50 µM, B), blebbistatin (30 µM, C), or brefeldin A (10 µg/ml, D). Increasing probe in the cytoplasm reflects release of membrane-bound probes as PLC depletes the lipid pools. All measurements were performed with conventional confocal microscopy.

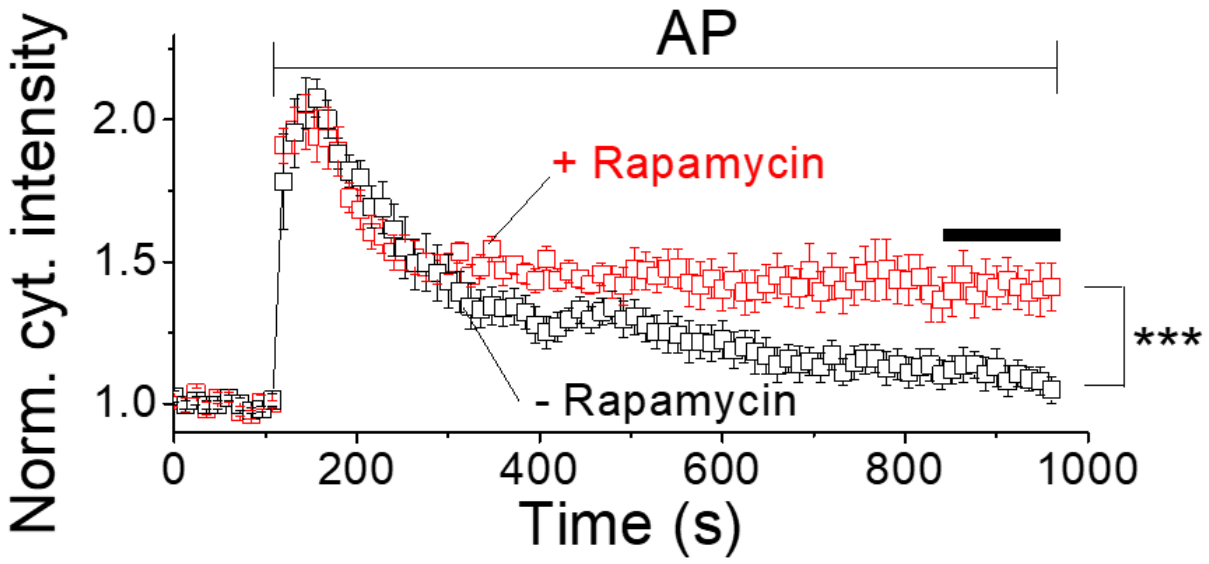

Fig. S3. The Golgi PI(4)P pool supports plasma membrane PI(4,5)P_2. Cells were transiently transfected with PAR2-dark, giantin-FRB-CFP, recruitable YFP-PJ Sac1, and PH-RFP. For real-time experiments, we first verified that cells were expressing all four constructs, and then PH-RFP and PJ-Sac1 were monitored every 12-s. Expression of PAR2-dark at the plasma membrane was checked with Alexa647-conjugated PAR2 primary antibody. Rapamycin was added for at least 6 min before 100 µM AP treatment. The time course of normalized cytoplasmic intensity of PH-RFP with (n = 8 cells) or without (n = 7 cells) rapamycin reflects depletion and recovery of PI(4,5)P_2 during AP application. Recovery was attenuated in cells where Sac1 had depleted the Golgi PI(4)P. A heavy bar indicates the points used for the t-test. ***, $P<0.005$.

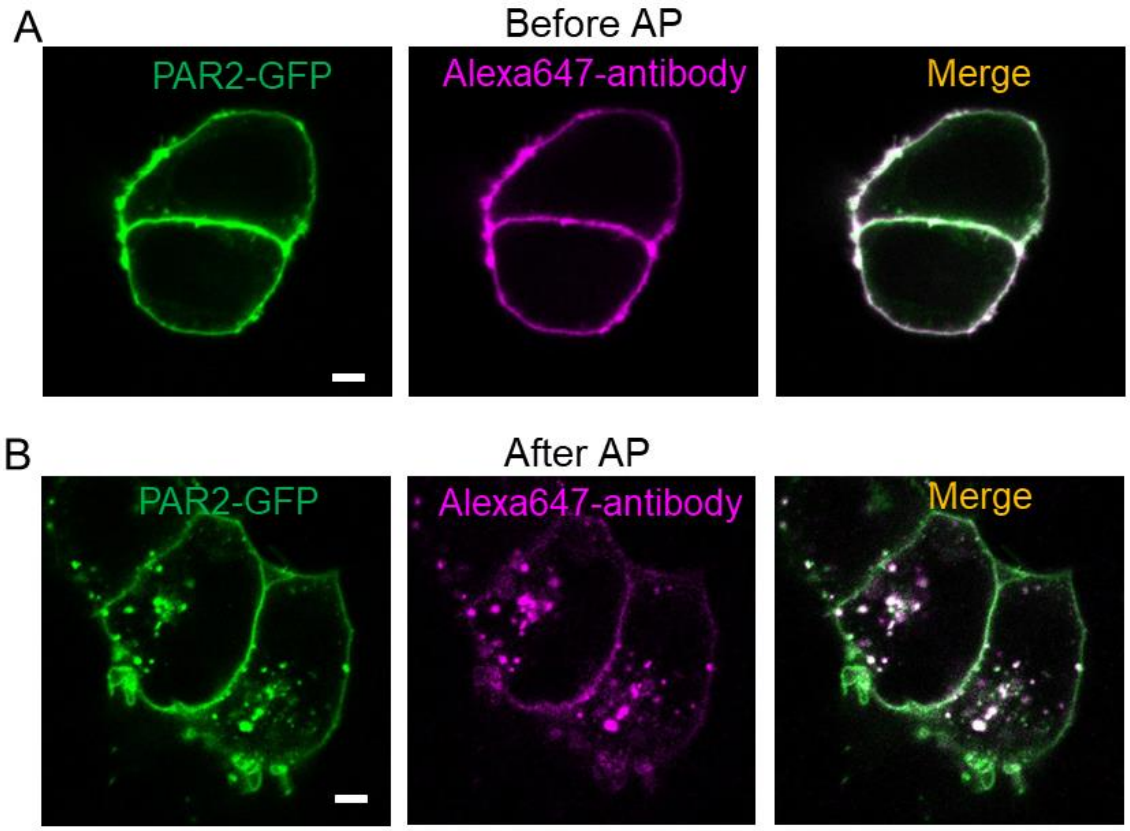

Fig. S4. Optical detection of PAR2 internalization. Cellular relocation of PAR2-GFP was seen by movement from the plasma membrane into the cytoplasm of both the GFP label and of labeled primary antibodies for PAR2. Cells were fixed before (A) or after (B) treatment with 100 µM AP for 1 h. Scale bar, 2 µm. PAR2-GFP and Alexa647-labeled PAR2 primary antibody were detected using two optical channels in a confocal microscope. The Alexa647-PAR2 antibody was used to quantify internalization of receptors unless stated otherwise.

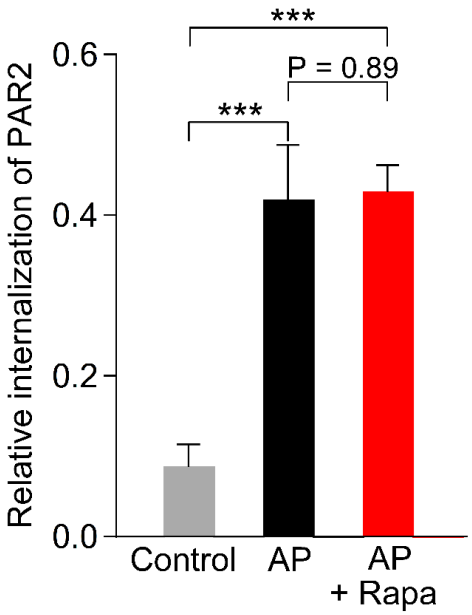

Fig. S5. No effect of rapamycin itself on PAR2 internalization. To estimate internalized PAR2, the fluorescence intensity of Alexa647-PAR2 antibody in the cytoplasm was compared to the intensity in the whole cell. Cells were treated with no addition ('Control', n = 14 cells), or with 100 μM AP ('AP', n = 12 cells) or 5 μM rapamycin following AP ('AP+Rapa', n = 7 cells). No recruitable enzymes were expressed in these cells. ***, P<0.005.

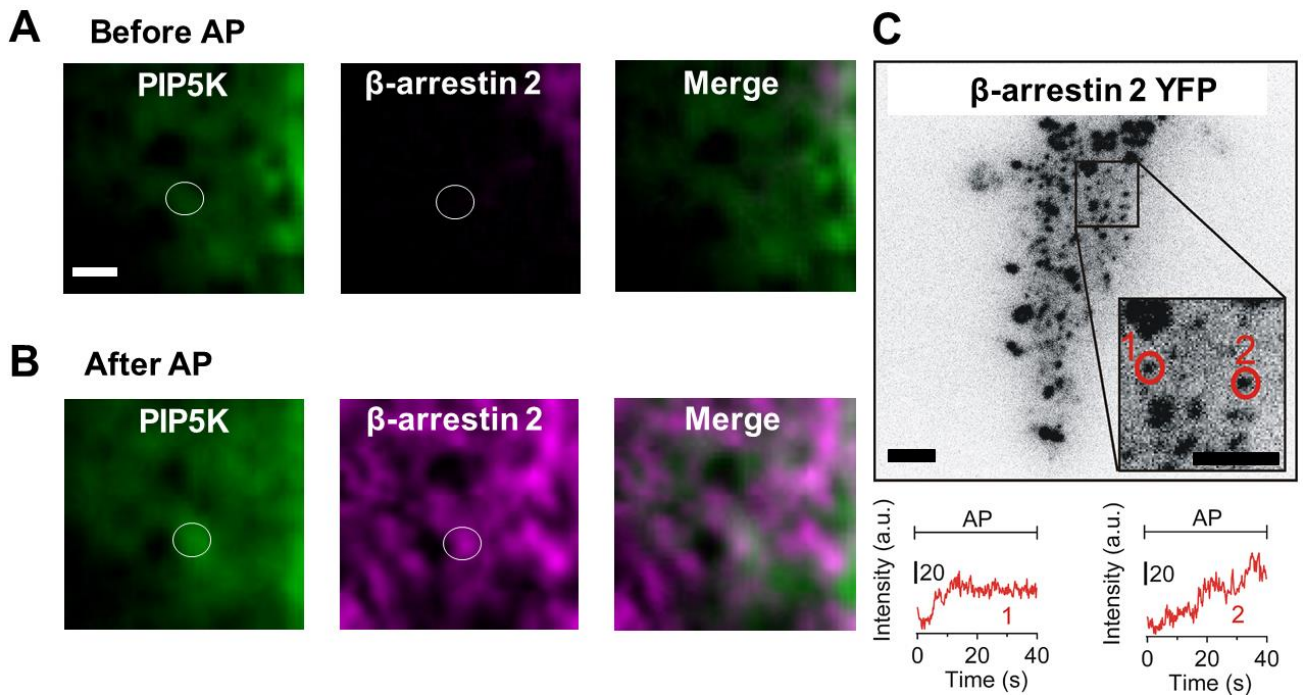

Fig. S6. Recruitment of PIP5K-Iγ into β-arrestin 2 clusters. GFP-PIP5K-Iγ and β-arrestin-2-mRFP transfected cells were imaged with two-color conventional TIRF microscopy (A-B). Scale bar, 2 μm. The TIRF panels show a region of interest (oval) from a single cell. Six images were averaged for each condition. The images in B were obtained 5-6 min after AP treatment. Most of the PIP5K-Iγ and β-arrestin 2 were expressed on the plasma membrane and in the cytoplasm, respectively. After adjustment of contrast to remove cytoplasmic signals for β-arrestin 2, we saw arrestin clusters. A region of interest was marked with a white circle based on the arrestin clusters for measuring recruitment of PIP5K-Iγ into arrestin clusters induced by AP treatment. (C) To see β-arrestin 2 clustering more clearly during AP treatment, cells were transfected with a 10-times lower amount of β-arrestin-2-YFP (0.05 μg cDNA) than had been used for β-arrestin-2-mRFP together with 0.1 μg PAR2-dark cDNA and viewed with single-molecule TIRF microscopy. Two local clusters of β-arrestin-2-YFP are marked 1 and 2. Their representative β-arrestin-2-YFP time courses are presented in red. Scale bars, 4 μm in whole-cell image and 2 μm in enlarged image.

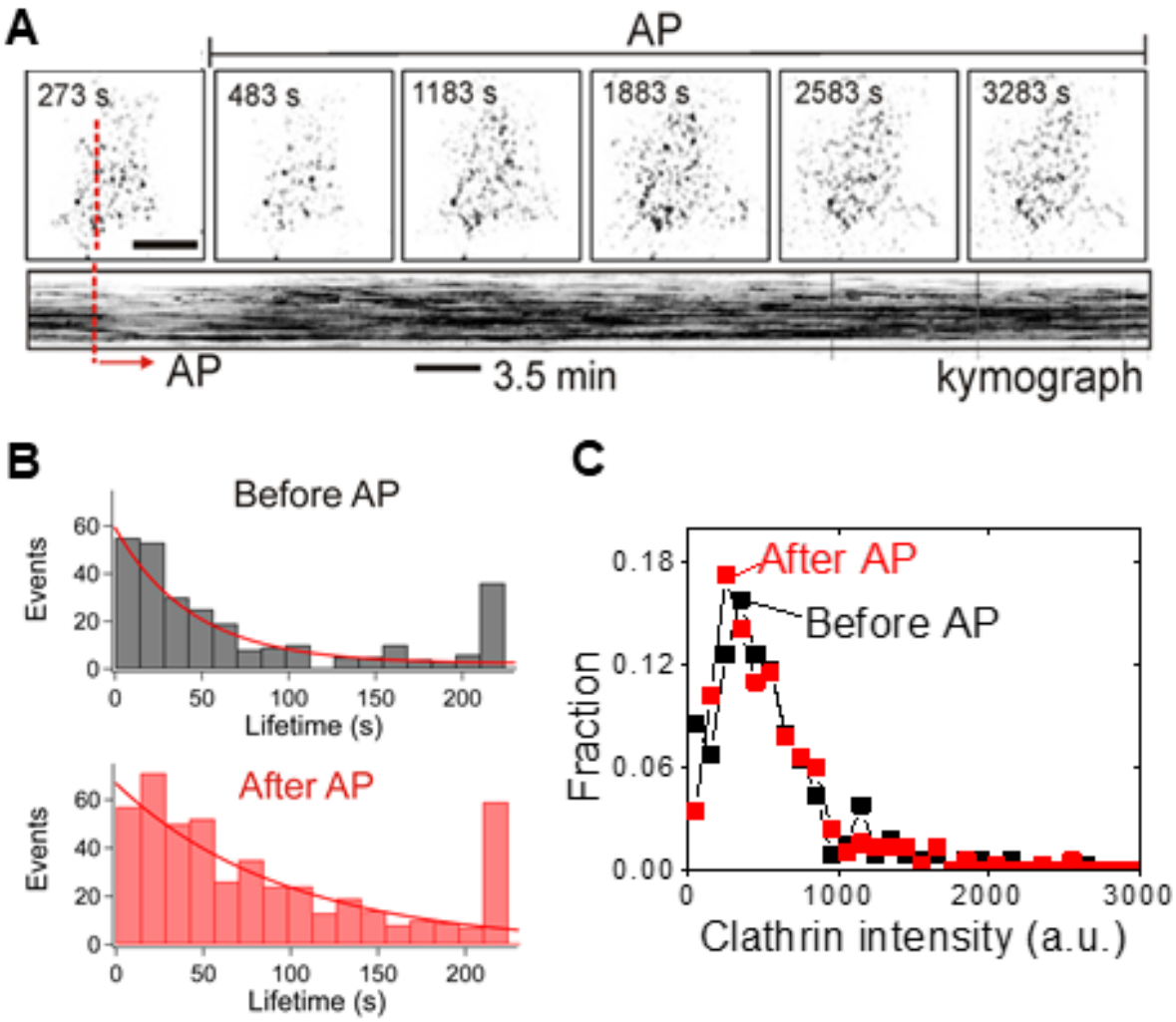

Fig. S7. Dynamic turnover of CCP in conventional TIRF microscopy. Cells were transfected with PAR2-GFP (0.5 μg cDNA) and clathrin-DsRed (0.5 μg cDNA). (A) TIRF images of CCP displayed at the different time points. Scale bar, 12 μm. The red line on the first image indicates where we scanned the stacked images to generate the CCP kymograph below. Kymograph time axis is horizontal with AP starting at the beginning of the arrow. The time interval for imaging was 7 s. (B) Lifetime of CCPs at the cell surface before AP treatment (top, analyzed for 30 frames = 210 s) and after 100 μM AP treatment (bottom, analyzed for 30 frames = 210 s) at 2,800 s. The histogram was binned in 14-s bins. The last bars indicate the sum of non-dynamic CCPs (plaques) that are a relatively minor portion compared to the dynamic CCPs. (C) Intensity distribution of individual CCPs before and after AP treatment.

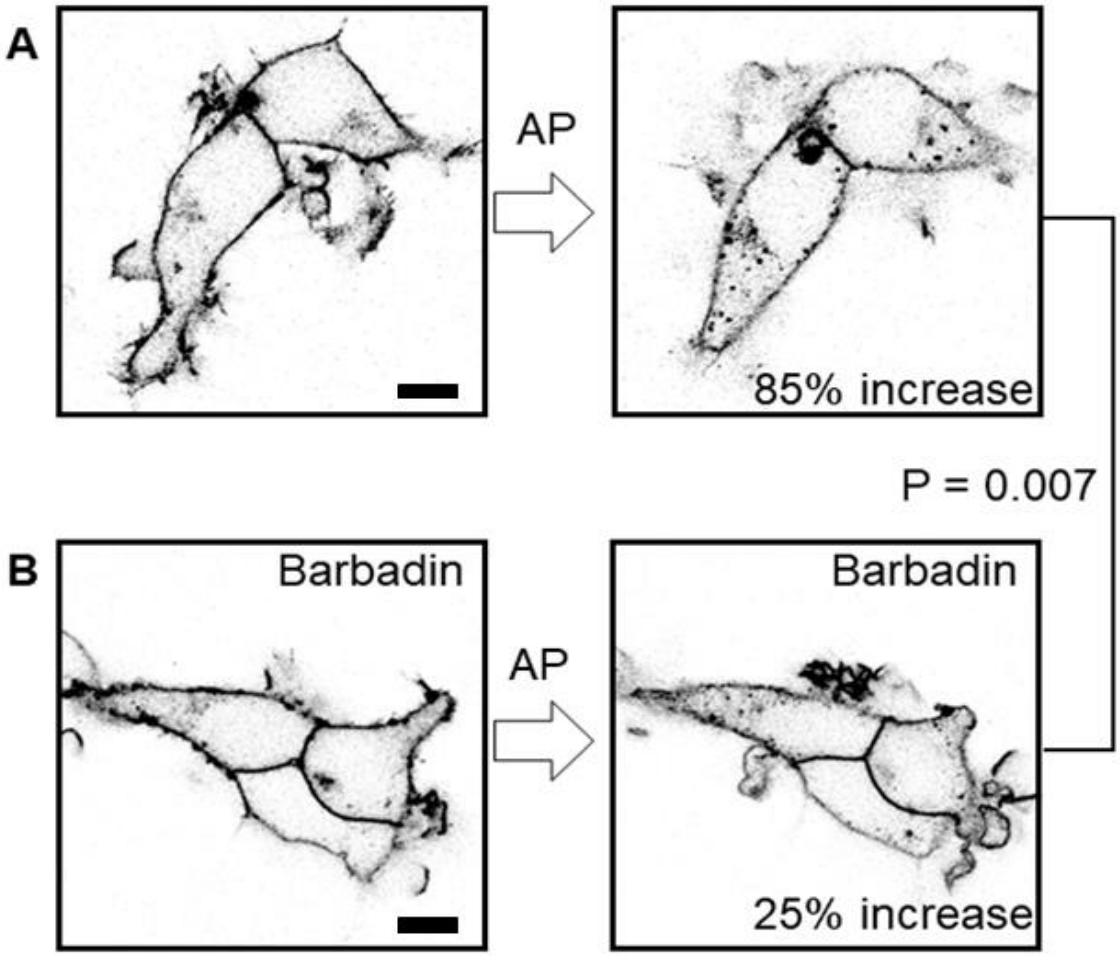

Fig. S8. Barbadin, a blocker of β-arrestin-AP2 interactions, attenuates PAR2 endocytosis. Cells were transfected with PAR2-GFP (0.5 µg cDNA) and PH-RFP (0.25 µg cDNA). (A-B) Inverted-contrast confocal images of endocytosis of GFP-tagged PAR2 receptors induced by 100 µM AP treatment and measured in the absence (A) or presence (B) of barbadin (50 µM). Cells were pretreated with barbadin for 5-10 min before AP addition. The endocytosis was normalized by the value before AP treatment (1.85 ± 0.1, in n = 4 cells without barbadin *vs.* 1.25 ± 0.12, in n = 5 cells with barbadin). P = 0.007. Scale bar, 4 µm.

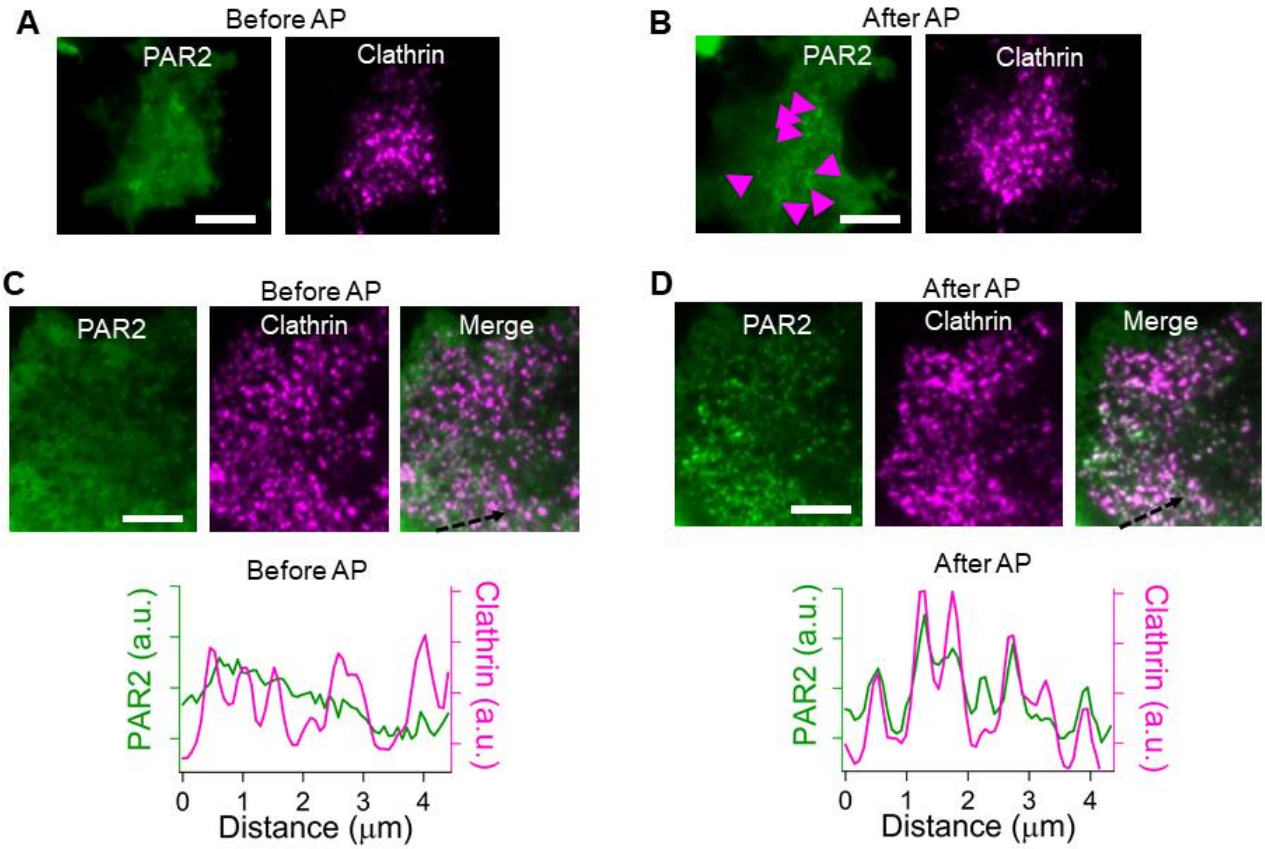

Fig. S9. PAR2 clustered at CCPs. (A-B) TIRF microscope images for PAR2-GFP and clathrin-DsRed obtained at time zero before AP (A) and after 46 minutes of AP treatment (B). The magenta arrowheads indicate clustered PAR2 receptors in CCPs after AP treatment (B, left). PAR2-GFP (0.5 μg cDNA) and clathrin- DsRed (0.5 μg cDNA) were transiently overexpressed. (C-D) TIRF microscopy with low density PAR2 and clathrin. Three strategies increased the contrast of clustering of PAR2-GFP around CCP: (i) low concentrations of PAR2-GFP cDNA (0.05 μg) and clathrin-DsRed cDNA (0.05 μg) were transiently transfected, (ii) the 488 and 561 nm laser powers were minimized to reduce photobleaching of GFP and DsRed, and (iii) 200 images were averaged to increase the signal-to-noise ratio. Nearly all CCPs were clustered with PAR2 receptors after AP treatment for 1 hour. From to the line scan analysis marked by dashed black arrows at the bottom of the merged images (C-D), we observed increased clustering of PAR2 with CCPs after AP treatment (D, bottom) compared to before AP (C, bottom). Scale bars, 10 μm (A-B) and 4 μm (C-D).

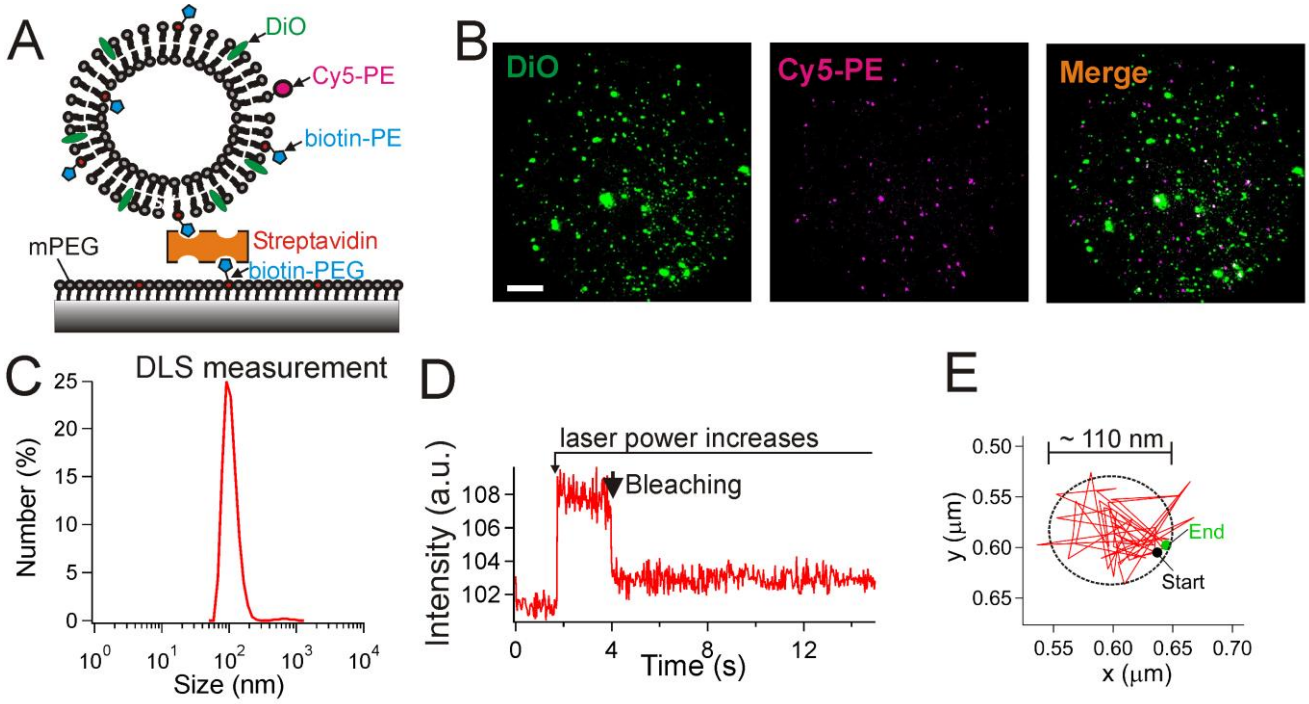

Fig. S10. Reconstitution of liposomes including Cy5-PE and DIO lipid dye. (A) Scheme of immobilization of POPC/biotin-PE/DiO/Cy5-PE liposome on PEG/streptavidin-coated glass slide for single-molecule TIRF experiments (See *SI Appendix* Methods and Materials: POPC liposome reconstitution with Cy5-PE). (B) Fluorescence images of DiO and Cy5-PE labeled POPC/biotin-PE liposomes. Scale bar, 5 μm. (C) Dynamic light scattering (DLS) assay to estimate the size of suspended liposomes. (D) Time course of fluorescence during a single photobleaching step of Cy5-PE (arrow). Excitation laser power was increased from 10 to 100 mW to bleach the Cy5 dye on a liposome. Background signal was not subtracted. (E) Single-molecule tracking of Cy5-PE in a liposome. Sampling interval was 50 ms for D and E.

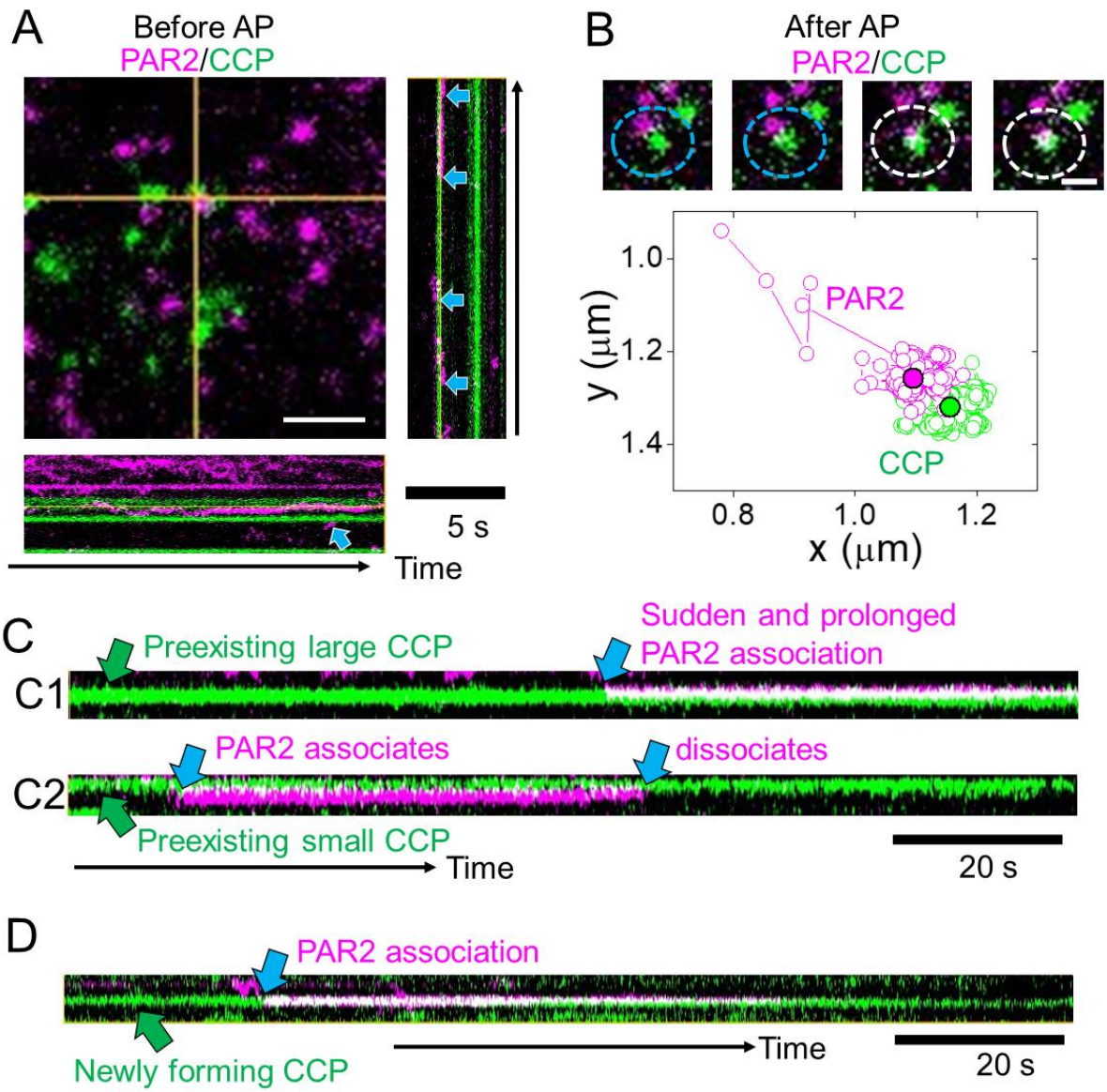

Fig. S11. Single-molecule, two-color TIRF images and dwell-time analysis of PAR2 interactions with CCPs using kymographs. Cells were transiently transfected with PAR2-dark (0.1 μg) and SNAP-clathrin (0.05 μg) cDNAs. PAR2 receptors were labeled extracellularly with Alexa647-PAR2 antibody before addition of the PAR2 agonist AP. A high concentration (1 mM) of AP was used here to maximize the fraction of ligand-bound receptors. Representative data before (A) and after (B) AP treatment. Scale bars: 1.5 μm (A), 0.3 μm (B). (A) TIRF image and kymograph projections of PAR2 (magenta) and clathrin (green) positions over time (black arrows indicate direction of time). The merged TIRF images at the center with scale bar is the first image of the time series. The yellow vertical and horizontal lines indicate scan lines used for generation of the kymographs and analysis of dwell times of receptor binding to the CCPs. Blue arrows in A point to brief transient binding of PAR2 receptors to CCPs before AP. (B) A series of four TIRF images taken at 100 ms intervals at the moment when a PAR2 receptor (magenta) binds to a CCP (green) indicated by dashed circles after AP application (top images). Single-molecule tracking traces of the PAR2 and CCP are shown below. These traces were used in Fig. 6B. Scale bar, 0.2 μm. Total recording time was ~2-5 min for different experiments. In this example, it was 110 s. (C) Kymograph records after AP showing PAR2 diffusing around a CCP and then suddenly forming an interaction (blue arrows) with a preexisting CCP (green arrows). The example in C1 was from panel B.

1,100 frames were used for the kymographs. The blue arrow shows a long association of PAR2 with the intense green CCP (“preexisting large CCP”). The intensity of CCP reflects size of CCP. Blue arrows in C2 indicate association and dissociation of PAR2 with a dim green CCP (“preexisting small CCP”). (D) Same for a newly forming CCP.

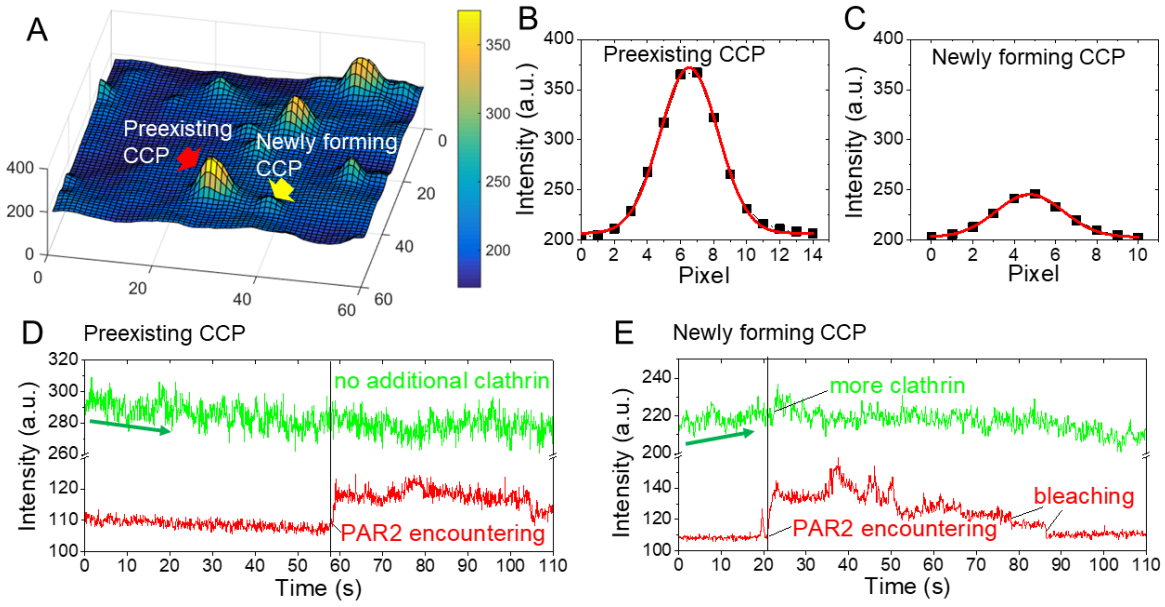

Fig. S12. Comparison of preexisting and newly forming CCPs after PAR2 activation. (A) Topographic surface plot of clathrin intensity generated from a single-molecule TIRF image showing preexisting (red arrow) and newly forming CCPs (yellow arrow). The x- and y-axes are in units of pixels (pixel size = 76 nm). The z-axis is in arbitrary units of intensity. This plot was constructed using Matlab. (B-C) Line-scan intensity profiles of two of the CCPs in A. Pixel size, 76 nm. The preexisting CCP has ~4-fold higher intensity than the newly forming CCP. (D-E) Time course intensity traces of PAR2 (red) as it binds to a CCPs (green). The green arrows under the clathrin traces showed decrease or increase of clathrin intensities in the CCPs. In the preexisting CCP, the clathrin intensity slowly decreased by photobleaching (D). In contrast, the newly-forming CCP intensity gradually increased due to accumulation of newly joining clathrins (E), although it also had parallel photobleaching. When the receptor was encountered, we observed a small intensity fluctuation in E ("more clathrin") compared to the preexisting CCP case which has no additional intensity change in D ("no additional clathrin"). The intensity traces were not corrected for background.

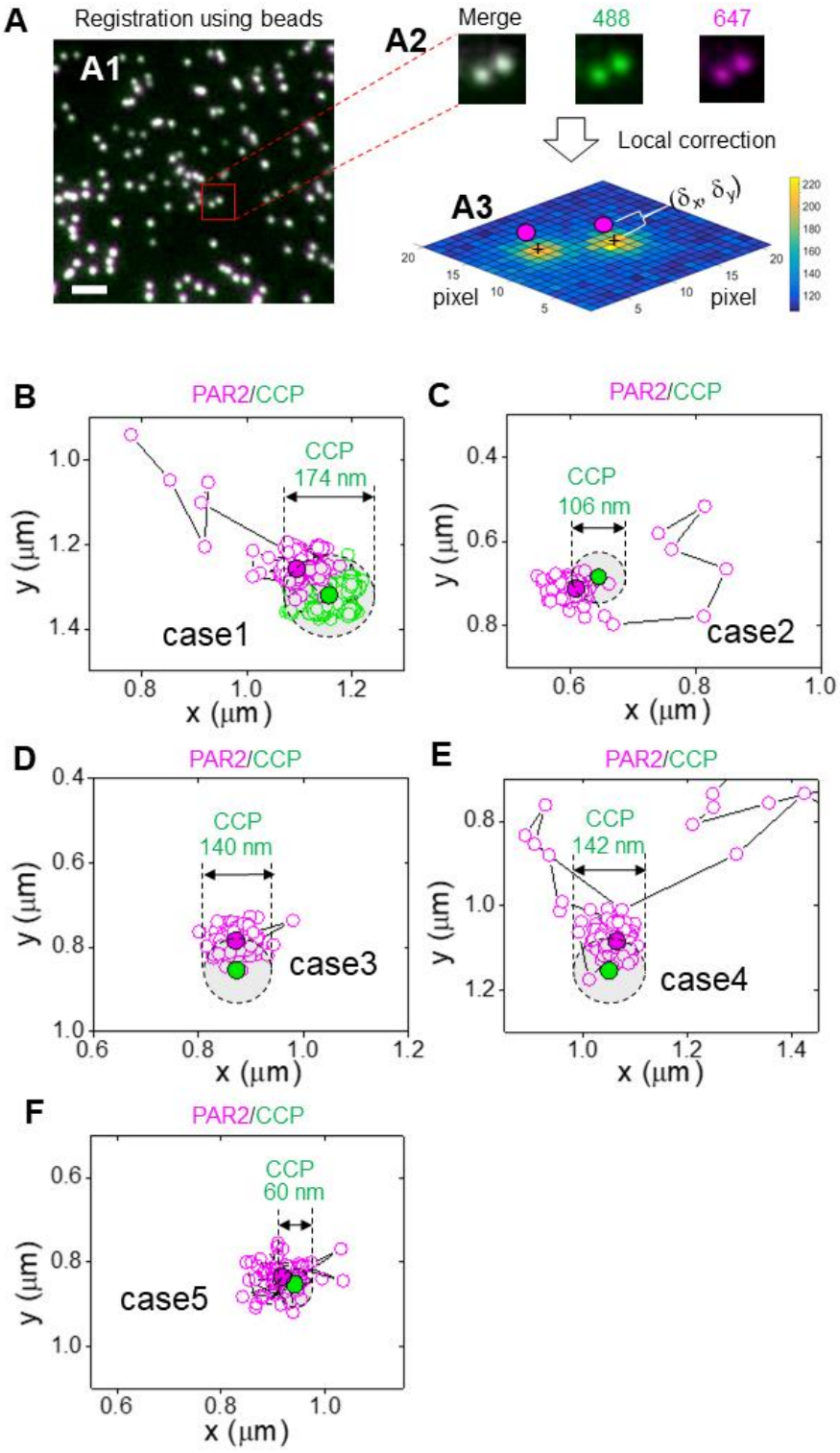

Fig. S13. Registration and local correction of single-molecule tracking. The steps involved in this calibration are: (i) to average multiple images to increase signal-to-noise ratio, (ii) to localize spots by fitting point-spread functions, and (iii) to correct registration errors and local errors using images of 200 nm multicolor beads as reference. (A1) Superimposed images of 200 nm multicolor beads excited by a 488 nm laser and emission collected at 525 and 700 nm. Scale bar, 1.5 μm. A global translation correction of registration of the two-color images has been applied. (A2) Magnified portions of the images in A1,

focusing on the red rectangular region in A1. (A3) The image of the green channel in A2 was rendered as a heat map using Matlab to show the intensity profiles of two beads with centers marked as crosses. Each pixel is 76 nm. In addition, two magenta filled circles have been drawn over the image to represent positions of the beads in the magenta channel. The local differences of x and y in the two channels are designated δx and δy, the local errors. The error of the magenta circles in this diagram is exaggerated and arbitrary to display the definition of terms better. The normal error and the actual error in A2 are much smaller. This local correction was calculated from bead images taken after the imaging the biological specimen, by selecting positions on the camera sensor that overlapped with that of the biological image to be corrected. (B-F) Representative trajectories of single PAR2 receptors (open magenta symbols) diffusing in the vicinity of CCPs (green symbols). These traces were corrected with the registration and local error-correction protocols. The filled magenta circles indicate the center of the final stable position of the PAR2 receptor once bound. If the receptors attach to the edge of CCPs, the center-to-center distance between immobilized receptor and CCP would be the effective radius of the CCP. The indicated diameter is twice this effective radius.

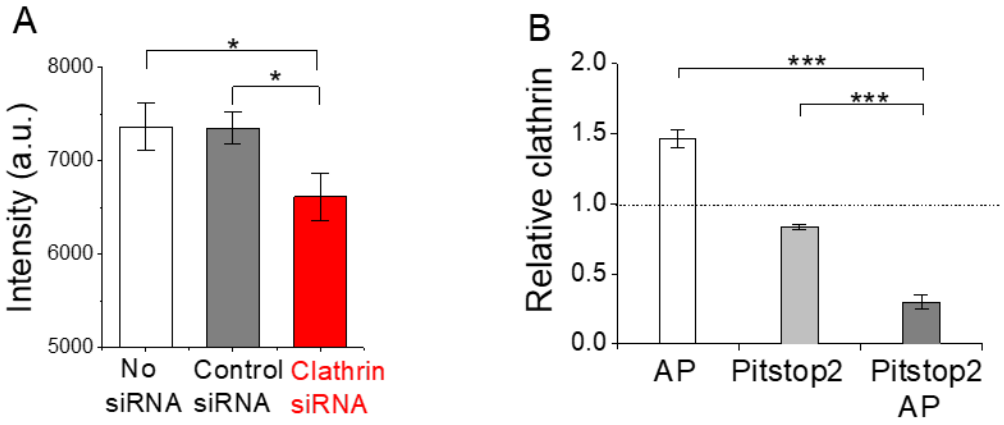

Fig. S14. Effect of clathrin heavy chain siRNA and Pitstop2. (A) Knock-down of clathrin heavy chains using siRNAs. The clathrin heavy chain was labeled with Alexa647 conjugated primary antibody in fixed specimens and its intensity was measured by conventional confocal microscopy (See SI *Appendix* Methods and Materials for protocol). No siRNA (n = 37 cells), Control siRNA (n = 26 cells), and Clathrin siRNA (n = 33 cells). *, P<0.05. (B) Normalized clathrin-DsRed intensity at the plasma membrane relative to unstimulated control cells showing that AP increased and AP plus pitstop2 decreased membrane clathrin. Clathrin-DsRed intensity at the plasma membrane was measured by TIRF microscopy. Cells were transiently transfected with PAR2-GFP (0.7 µg cDNA) and clathrin-DsRed (0.5 µg cDNA). The AP bar (n = 7 cells) is from one set of live cell experiments comparing after AP (60 min) to before AP. The pitstop2 results are from a second set of experiments. After a control measurement, Pitstop2 (25 µM) was applied for 5-10 min ('Pitstop2', n = 7 cells). Then 100 µM PAR2 agonist (AP) was applied for 60 min in the presence of the Pitstop2 ('Pistop2/AP', n = 7 cells). All intensities were corrected for the background signal outside the cells. ***, P<0.005.

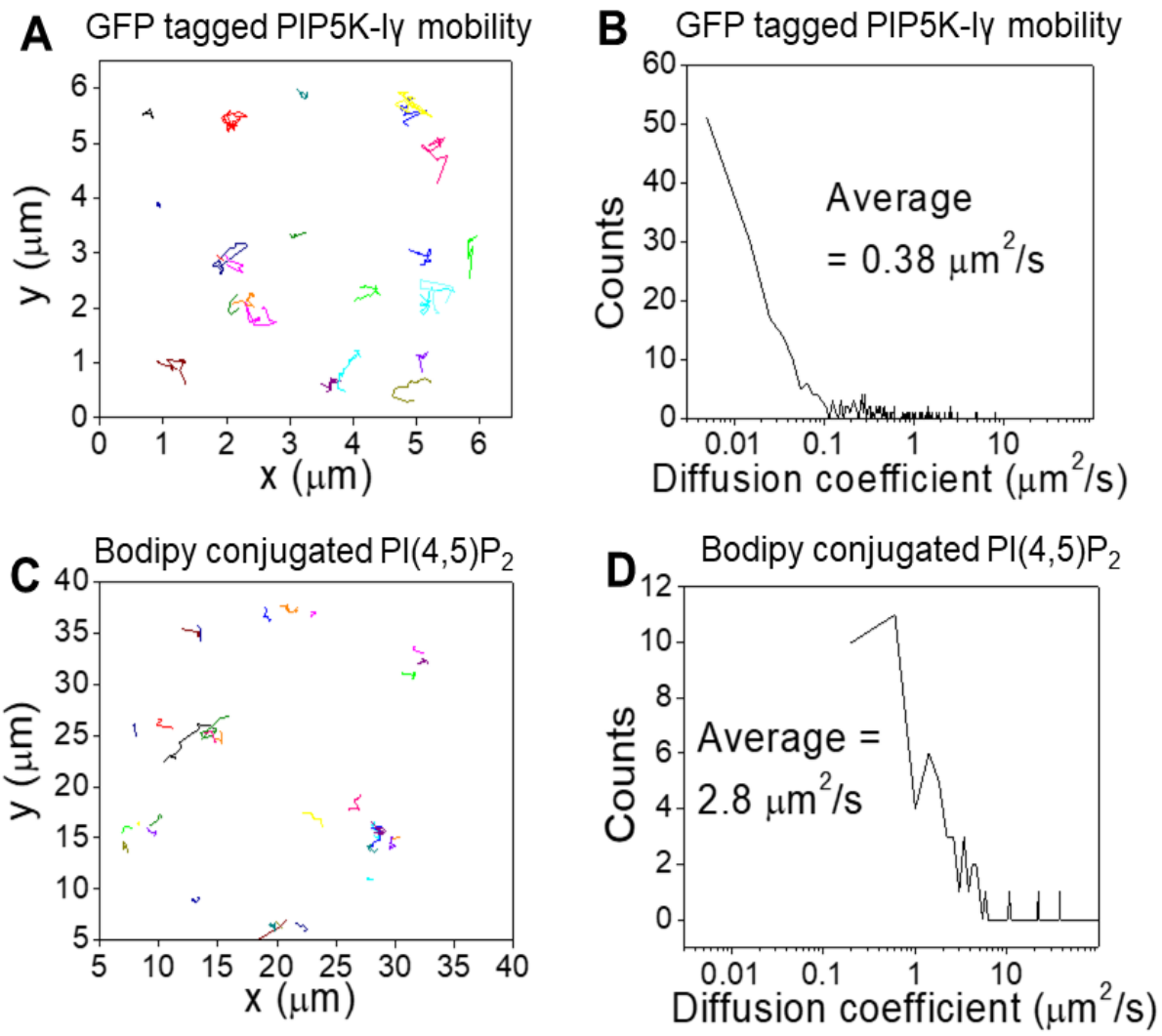

Fig. S15. Mobility of GFP tagged PIP5K-Iγ protein at the plasma membrane compared with Bodipy conjugated PI(4,5)P_2 lipid in artificial membranes. (A-B) Cells were transiently transfected with PAR2-dark (1 μg cDNA), GFP-PIP5K-Iγ (0.01 μg cDNA) and clathrin-DsRed (0.05 μg cDNA). For these single-molecule tracking experiments, the amount of GFP-PIP5K-Iγ cDNA was ~50 times lower than that for conventional TIRF and confocal microscopy. (A) Single-molecule trajectories of 20 exemplar diffusing PIP5K-Iγ molecules (different colors) measured 60 min after application of PAR2 agonist (AP). (B) Distribution of diffusion coefficients of the GFP-PIP5K-Iγ after AP treatment. The mean diffusion coefficient was 0.38 ± 0.06 $\mu m^2/s$ (n = 238 molecules). (C-D) Mobility of Bodipy conjugated PI(4,5)P_2. Bodipy conjugated PI(4,5)P_2 (100 ng/ml) was introduced onto a POPC-based lipid bilayer. The Bodipy was conjugated to the one of acyl chains of PI(4,5)P_2, not on the inositol head group. (C) Single-molecule trajectories of 32 exemplar diffusing Bodipy-PI(4,5)P_2 molecules (different colors) (D) Distribution of diffusion coefficients of Bodipy-PI(4,5)P_2. The average diffusion coefficient was 2.8 ± 0. 8 $\mu m^2/s$ (n = 56 molecules). The diffusion of the lipid molecules was much faster than that of plasma membrane PIP5K-Iγ complexes.

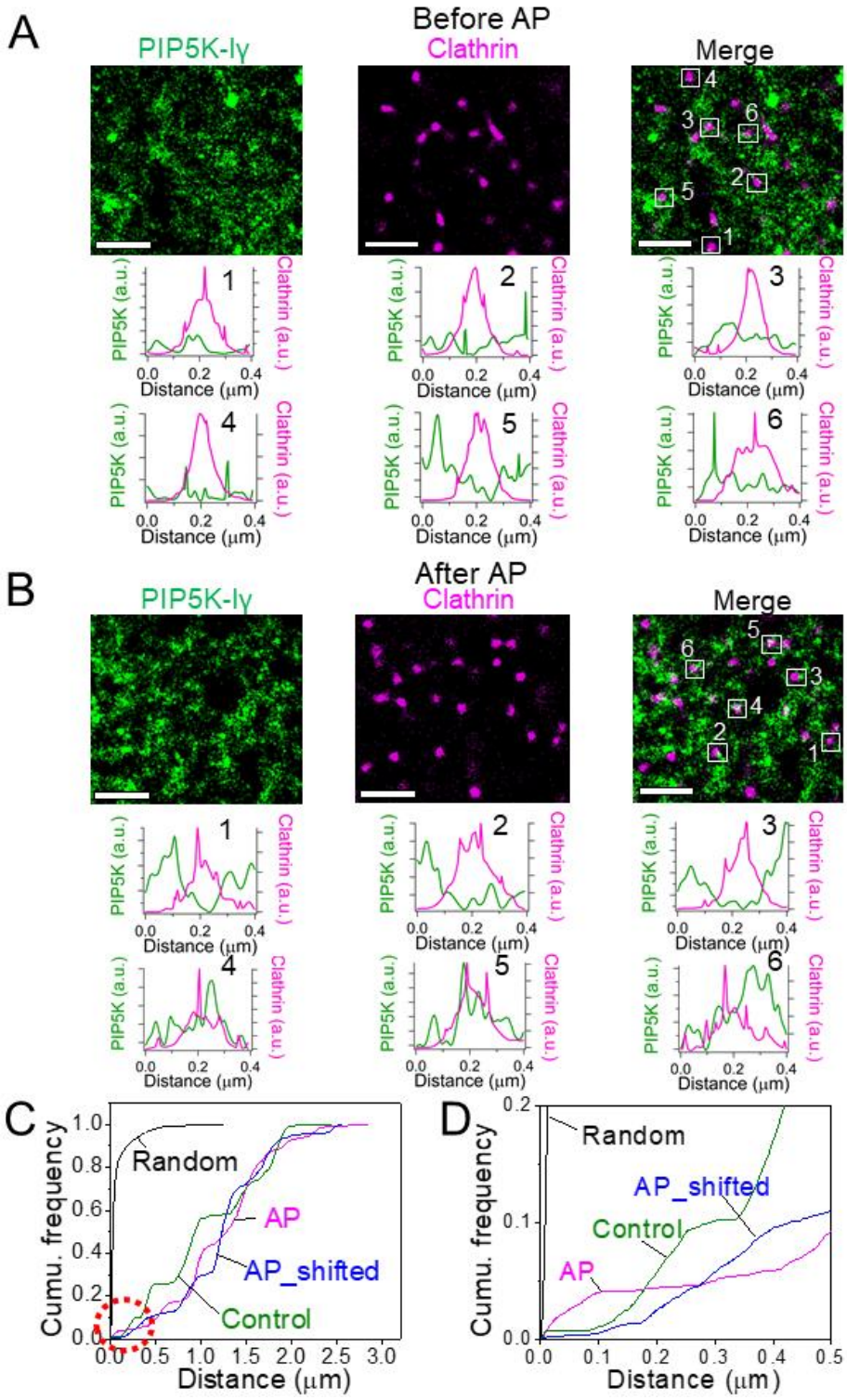

Fig. S16. **Mapping of PIP5K-Iγ around CCPs.** Cells were transiently transfected with GFP-PIP5K-Iγ (0.01 μg), clathrin-DsRed (0.05 μg) and PAR2-dark (0.8 μg). (A) Single-molecule localization and reconstruction microscopy density-mapped images of PIP5K-Iγ (GFP-PIP5K-Iγ) around CCPs (clathrin-DsRed) before AP treatment. Scale bars, 1 μm. The data were analyzed with ThunderSTORM in ImageJ. Six representative regions of interest (ROIs) marked by small white boxes before (A) or after AP treatment (B) were used for measuring distributions of PIP5Ks around a single CCP. Distributions are shown below

the images. Before AP, most PIP5K-Iγs were not localized with CCPs. (B) After AP, PIP5K-Iγs were either close by the outer edges of CCPs (ROIs 1,2,3) or spread within the CCPs (ROIs 4,5,6). (C) Normalized cumulative frequency ('Cumu. Frequency') plot of nearest neighbor distance (NND) of PIP5K-Iγ molecules to CCPs. NND measures the distance of the nearest CCP from the center of each PIP5K-Iγ. The algorithm also generates a random case automatically, plotting the distance to spots placed randomly within a single CCP. Three different conditions: Control (before AP, green), AP (during AP, magenta), and AP_shifted (blue) were plotted. AP_shifted means that the CCP image obtained from AP application was shifted 320 nm on the x-axis and 400 nm on the y-axis relative to the PIP5K-Iγ image to simulate an uncorrelated distribution. (D) Enlarged plot of the red dotted circle region in C.

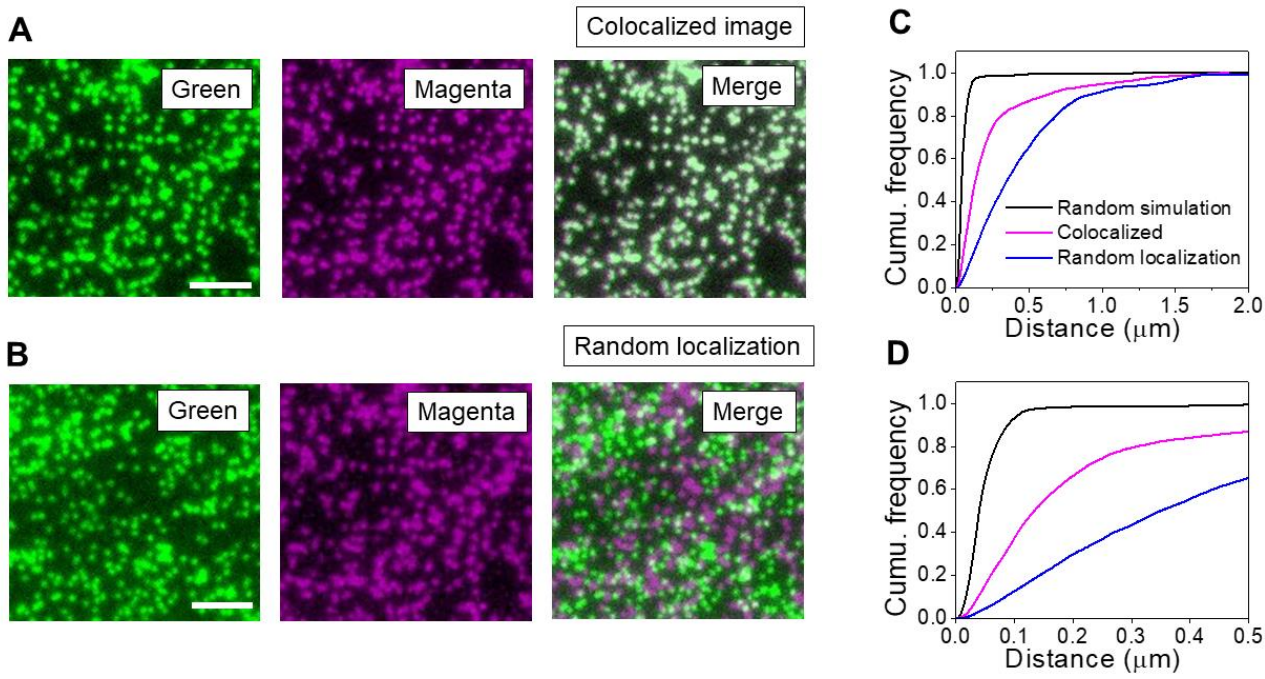

Fig. S17. Tests of nearest neighbor distance (NND) analysis using 200 nm multicolor beads. Beads were immobilized with 1M Tris-HCl (pH = 8.0) solution on a plasma-cleaned glass surface. The beads were excited by a 488 nm laser, and emission light was collected by two different bandpass filters (green = 525 nm, Magenta = 600 nm). (A-B) NND analysis was performed for two different simulated cases: completely colocalized (A) or randomly localized (B). The magenta images in (A) and (B) are same. The green image in (B) was switched for an image obtained from a different region of the same sample. Scale bars, 1 μm. (C-D) Plots of normalized cumulative frequency ('Cumu. Frequency'). Normalization provided by the routine, Statistics 2D/3D, in ImageJ removed the effect of variation of the number of spots. (C) Colocalization was from panel A (magenta line) and random localization was from panel B (blue line). The random simulation (black line) simulated a random distribution of green spots inside a single magenta region. (D) Expanded scale of C.

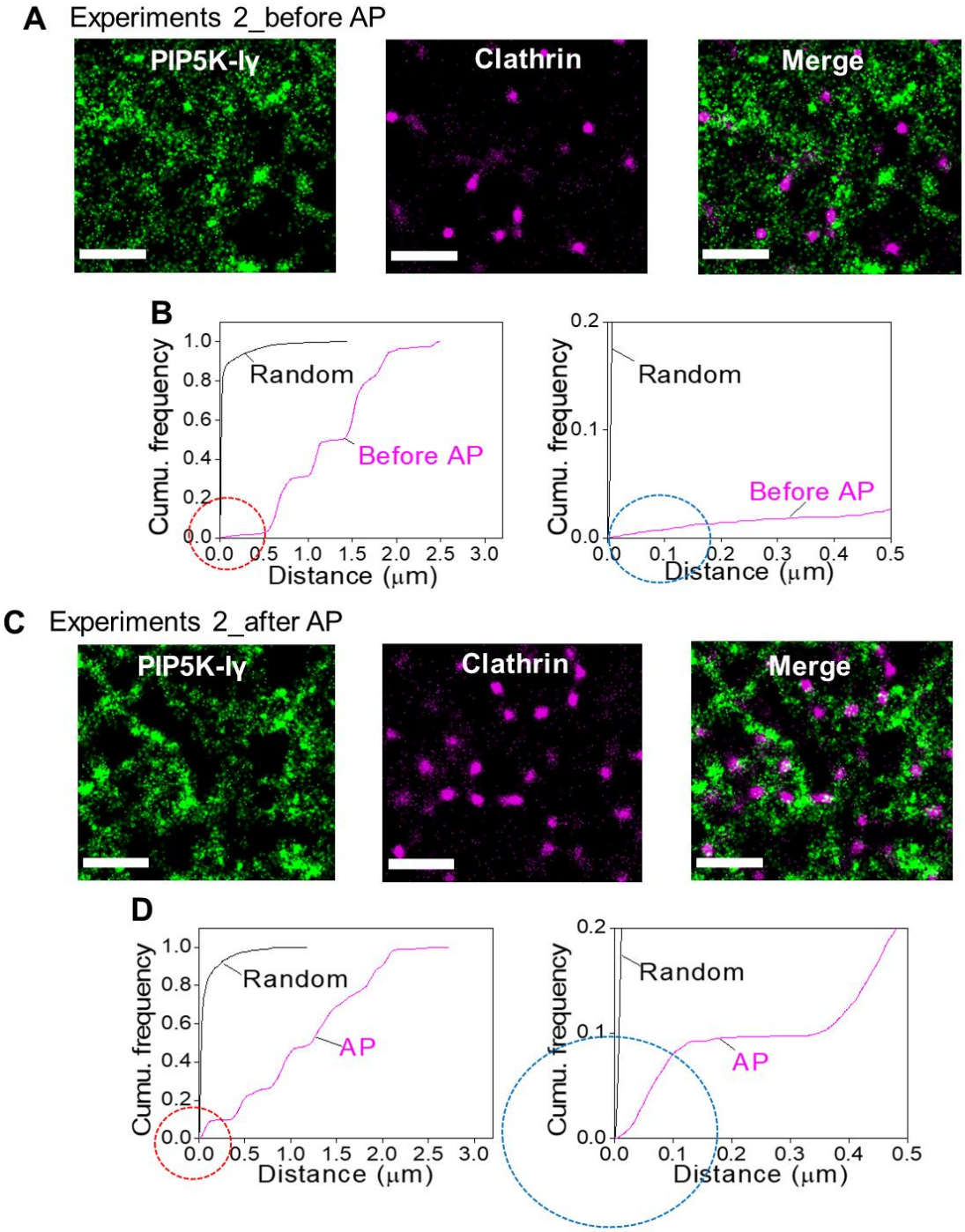

Fig. S18. Nearest neighbor distance (NND) analysis of PIP5K-Iγ around CCPs before (A-B) or after (C-D) AP treatment. Cells were transiently transfected with PAR2-dark (0.8 μg cDNA), GFP-PIP5K-Iγ (0.01 μg cDNA) and clathrin-DsRed (0.05 μg cDNA). (A) Single-molecule localization and reconstruction TIRF microscopy density-mapped images of PIP5K-Iγ (GFP-PIP5K-Iγ) around CCPs (clathrin-DsRed) before AP treatment. Scale bars, 1 μm. (B) Normalized cumulative frequency ('Cumu. Frequency') of NND before AP. Full plot on left and expanded scale of the red dashed circle region in C on right. (C-D) Same kinds of images and frequency plots after AP. The blue circles in the expanded scale indicate PIP5K-Iγ populations in CCPs.

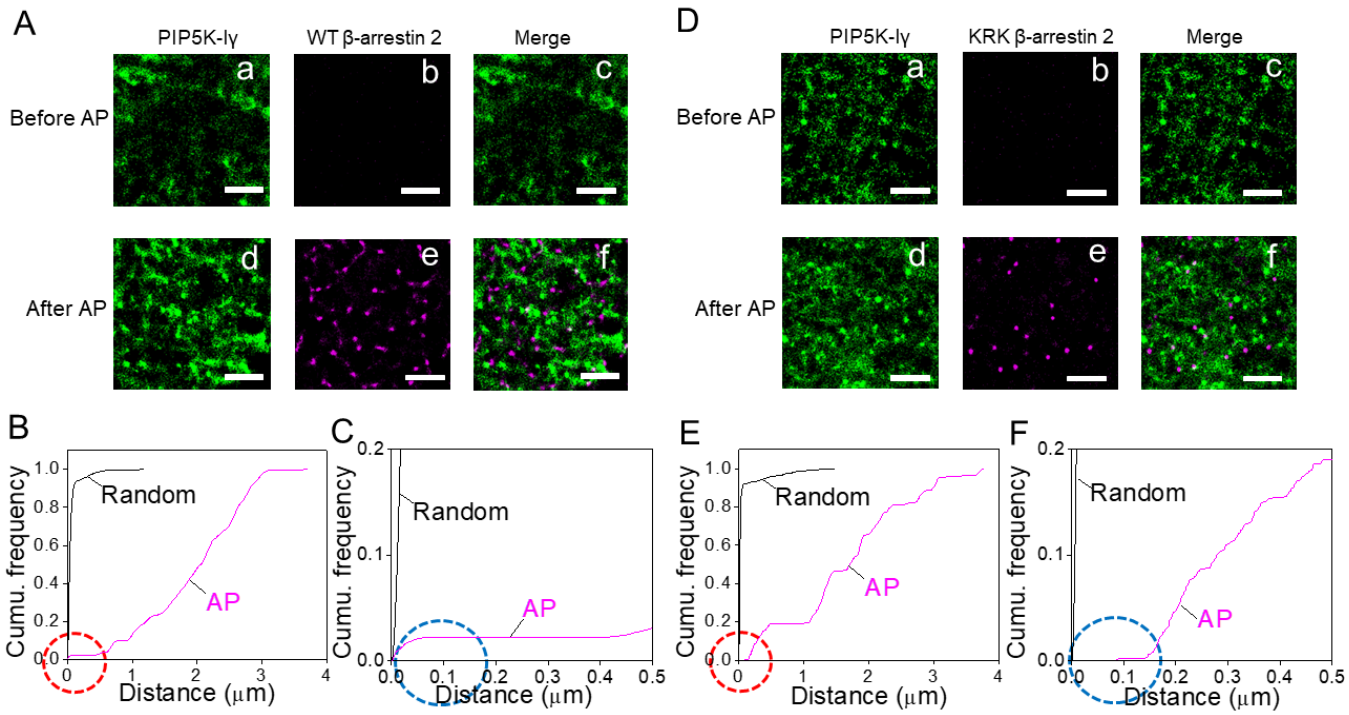

Fig. S19. Nearest neighbor distance (NND) analysis between PIP5K-Iγ and wild type (WT) β-arrestin 2 and between PIP5K-Iγ and KRK mutant β-arrestin 2. Cells were transiently transfected with: (A-C) PAR2-dark (1 μg cDNA), GFP-PIP5K-Iγ (0.01 μg cDNA) and wild type β-arrestin-2-mRFP (0.05 μg cDNA) or (D-F) PAR2-dark (1 μg cDNA), GFP-PIP5K-Iγ (0.01 μg cDNA) and KRK mutant β-arrestin-2-mRFP (0.2 μg cDNA). (A) Single-molecule localization and reconstruction TIRF microscopy density-mapped images. (B-C) Plot of normalized cumulative NND frequency ('Cumu. Frequency') with wild type β-arrestin-2-mRFP. The red dashed circle in B is enlarged in C. The area marked with a blue dashed line indicates PIP5K-Iγ inside β-arrestin 2 clusters. (D-F) Same images and plots for the KRK mutant β-arrestin-2-mRFP. Scale bars, 1 μm.

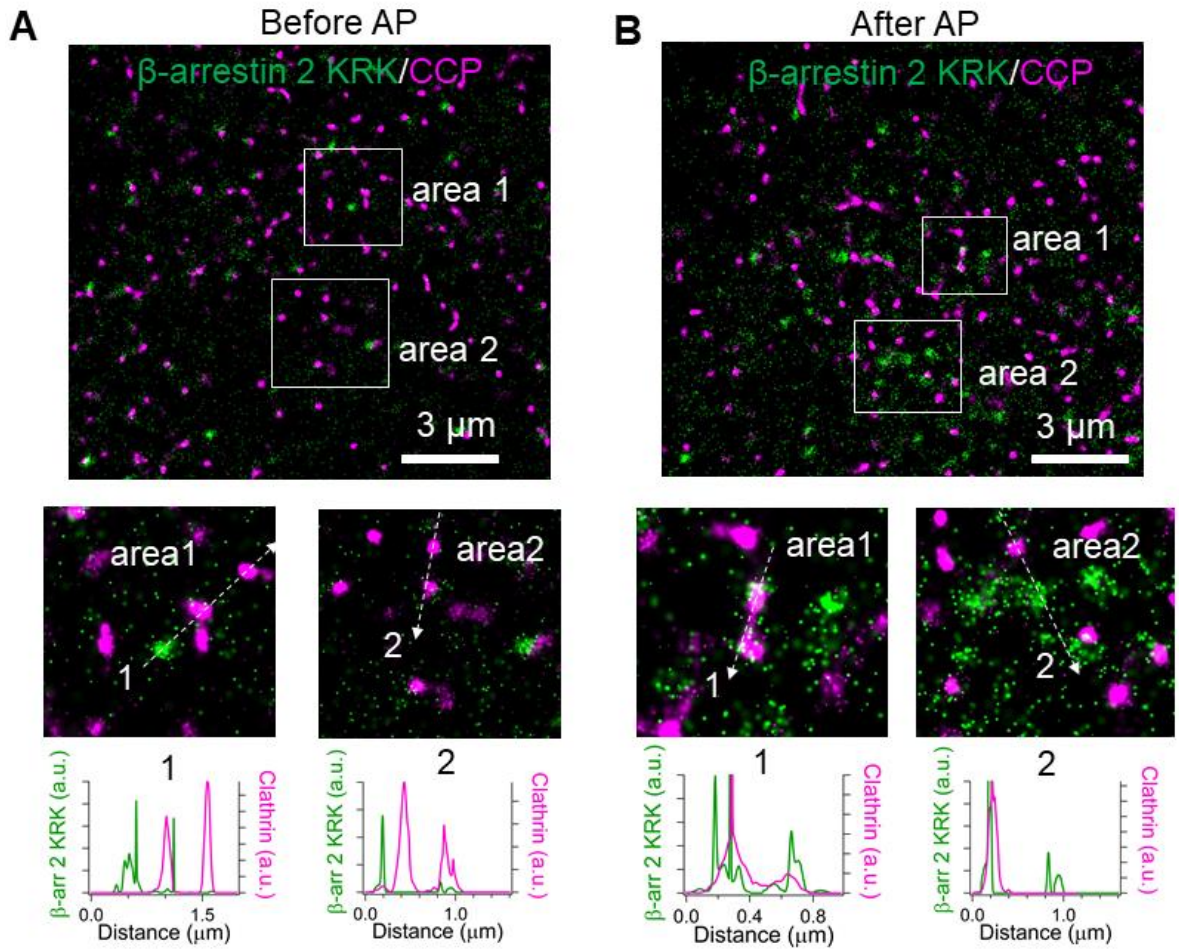

Fig. S20. Colocalization of the KRK mutant of β-arrestin 2 with CCP before (A) and after AP (B). PAR2-dark (1 μg cDNA), clathrin-DsRed (0.05 μg cDNA), KRK mutant β-arrestin-2-YFP (0.2 μg cDNA). Single-molecule localization and reconstruction TIRF microscopy to remove the background signals from cytosolic β-arrestins. Single-molecule analysis was done by ThunderSTORM in ImageJ. Roughly 3 μm x 3 μm regions of interest are marked and expanded below to visualize colocalization of KRK mutant β-arrestin 2 with CCPs. They were line-scanned along the white arrows. Before AP treatment, only a few KRK mutant β-arrestin 2 at the plasma membrane were located near CCPs. After 100 μM AP addition, the plasma membrane KRK mutant β-arrestin-2-YFP signal (green) was slightly increased. The arrestins were clustered by themselves without CCP or scattered randomly on the plasma membrane.

SI References

1. E.J. Dickson, J.B. Jensen, B. Hille, Golgi and plasma membrane pools of PI(4)P contribute to plasma membrane PI(4,5)P_2 and maintenance of KCNQ2/3 ion channel. *Proc. Natl. Acad. Sci. USA* **111**, E2281-E2290 (2014).
2. P. Delmas, B. Coste, N. Gamper, M.S. Shapiro, Phosphoinositide lipid second messengers: new paradigms for calcium channel modulation. *Neuron* **47,** 179-182 (2005).
3. J. de Barry et al., Functional implication of neuronal calcium sensor-1 and phosphoinositol 4-kinase-beta interaction in regulated exocytosis of PC12 cells. *J. Biol. Chem.* **281**, 18098-18111 (2006).
4. S. Miserey-Lenkei, G. Chalancon, S. Bardin, E. Formstecher, B. Goud, A. Echard, Rab and actomyosin-dependent fission of transport vesicles at the Golgi complex. *Nat. Cell Biol.* **12**, 645-654 (2010).
5. J. Lippincott-Schwartz, L.C. Yuan, J.S. Bonifacino, R.D. Klausner, Rapid redistribution of Golgi proteins into the ER in cells treated with brefeldin A: evidence for membrane cycling from Golgi to ER. *Cell* **56,** 801-813 (1989).
6. S.R. Jung et al., Contributions of protein kinases and β-arrestin to termination of protease-activated receptor 2 signaling. *J. Gen. Physiol.* **147**, 255-271 (2016).
7. G.R. Hammond, M.P. Machner, T. Balla, A novel probe for phosphatidylinositol 4-phosphate reveals multiple pools beyond the Golgi. *J. Cell Biol.* **205,** 113-126 (2014).
8. B.C. Suh, T. Inoue, T. Meyer, B. Hille, Rapid chemically induced changes of PtdIns(4,5)P_2 gate KCNQ ion channels. *Science* **314**, 1454-1457 (2006).
9. S.R. Jung, C. Kushmerick, J.B. Seo, D.S. Koh, B. Hille, Muscarinic receptor regulates extracellular signal regulated kinase by two modes of arrestin binding. *Proc. Natl. Acad. Sci. USA* **114**, E5579-E5588 (2017).
10. S.R. Jung, B. Hille, Optical approaches for visualization of arrestin binding to muscarinic receptor. *Methods Cell Biol.* **149**, 1-18 (2019).
11. S.R. Jung et al., Minimizing ATP depletion by oxygen scavengers for single-molecule fluorescence imaging in live cells. *Proc. Natl. Acad. Sci. USA* **115**, E5706-E5715 (2018).
12. D. Bucher et al., Clathrin-adaptor ratio and membrane tension regulate the flat-to-curved transition of the clathrin coat during endocytosis. *Nat. Commun.* **9**, 1109. Doi: 10.1038/s41467-018-03533-0 (2018).
13. B.L. Scott et al., Membrane bending occurs at all stages of clathrin-coat assembly and defines endocytic dynamics. *Nat. Commun.* **9**, 419 (2018).
14. S.R. Jung et al., Dynamic anchoring of the 3'-end of the guide strand controls the target dissociation of Argonaute-guide complex. *J. Am. Chem. Soc.* **135**, 16865-16871 Doi: 10.1021/ja403138d (2013).
15. M. Ovesny, P. Krizek, J. Borkovec, Z. Svindrych, G.M. Hagen, ThunderSTORM: a comprehensive image J plug-in for PALM and STORM data analysis and super-resolution imaging. *Bioinformatics*. **30**, 2389-2390 (2014).